Mapping the early steps in the pH-induced conformational conversion of the prion protein

Darwin O. V. Alonso*, Stephen J. DeArmond†, Fred E. Cohen‡, and Valerie Daggett*§

*Department of Medicinal Chemistry, University of Washington, Seattle, WA 98195-7610; and Departments of †Pathology (Neuropathology), and ‡Molecular and Cellular Pharmacology, University of California, San Francisco, CA 94143

Edited by Alan Fersht, University of Cambridge, Cambridge, United Kingdom, and approved January 4, 2001 (received for review November 22, 2000)

Under certain conditions, the prion protein (PrP) undergoes a conformational change from the normal cellular isoform, PrP^C, to PrP^{Sc}, an infectious isoform capable of causing neurodegenerative diseases in many mammals. Conversion can be triggered by low pH, and *in vivo* this appears to take place in an endocytic pathway and/or caveolae-like domains. It has thus far been impossible to characterize the conformational change at high resolution by experimental methods. Therefore, to investigate the effect of acidic pH on PrP conformation, we have performed 10-ns molecular dynamics simulations of PrP^C in water at neutral and low pH. The core of the protein is well maintained at neutral pH. At low pH, however, the protein is more dynamic, and the sheet-like structure increases both by lengthening of the native β-sheet and by addition of a portion of the N terminus to widen the sheet by another two strands. The side chain of Met-129, a polymorphic codon in humans associated with variant Creutzfeldt–Jakob disease, pulls the N terminus into the sheet. Neutralization of Asp-178 at low pH removes interactions that inhibit conversion, which is consistent with the Asp-178–Asn mutation causing human prion diseases.

PrP^C is a glycosylated, glycosylphosphatidylinositol-anchored component of the extracellular surface of neurons that appears to play a role in signal transduction (1). PrP^{Sc}, the misfolded isoform, is a β-sheet-rich, protease-resistant protein that causes fatal neurodegenerative diseases of the central nervous system in humans and other mammals (2, 3). Clinically, these diseases can exhibit sporadic, inherited, or infectious presentations. Neuropathologically, spongiform degeneration with astrocytic gliosis and extracellular deposits rich in the prion protein (PrP) are observed (4). Inherited disease maps exclusively to mutations in the PrP. Infectious disease is transmitted by PrP^{Sc}, which is chemically indistinguishable from PrP^C (5); however, their secondary, tertiary, and quaternary structures differ (6–10). PrP^C is monomeric, whereas PrP^{Sc} adopts a multimeric arrangement. Fourier transform infrared and CD spectroscopy studies indicate that PrP^C is highly helical (42%), with little β-sheet structure (3%) (8). In contrast, PrP^{Sc} contains a large amount of β-structure (43%) and less helical structure (30%). These results and others suggest that a conversion of α-helices to β-sheets is an essential feature in the formation of PrP^{Sc} from PrP^C.

Recombinant forms of human and murine PrP^C undergo a pH-dependent conformational change in the region of pH 4.4–6, with a loss of helix and gain of β-structure (11, 12). *In vivo*, conversion of $PrP^C \rightarrow PrP^{Sc}$ is a posttranslational process that appears to occur in an endocytic pathway (7, 13, 14). Caveolae-like domains have also been implicated in the conversion of wild-type protein (15, 16), and they appear to be acidic (17). Lower pH accelerates conversion in a cell-free conversion assay (10). Thus low pH may play a role in facilitating the conformational change that ultimately results in PrP^{Sc} formation.

Recent advances in NMR studies of recombinant nonglycosylated fragments of the PrP have produced several structures. The available mouse (18), hamster (19, 20), and human PrP structures (21) are very similar, as would be expected for sequences exhibiting >90% homology. They contain a C-terminal domain (residues 90–231) with three well-resolved helices and a short two-stranded β-sheet and an unstructured N-terminal region (residues 23–90), which becomes more structured with the addition of Cu(II) (22, 23) or a membrane environment (24). One obvious difference between the hamster, mouse, and human fragments is the N-terminal hydrophobic globule observed by James *et al.* in the 90–124 region of the hamster protein fragment containing residues 90–231 (19). This region is particularly interesting because mutations and transgenic studies implicate it in the conversion of $PrP^C \rightarrow PrP^{Sc}$. The 90–124 region is conformationally heterogeneous and is judged to be largely disordered by NMR at acidic pH (20). X-ray crystallographic studies of a peptide from this region bound to the 3F4 antibody demonstrate that residues 106–114 can form an Ω-loop (25). Follow-up NMR studies of full-length PrP indicate that there is a marked difference in flexibility and dynamic behavior between the N terminus (residues 23–124) and the folded core of the molecule, as probed by the heteronuclear ^{15}N-^{1}H nuclear Overhauser effect and described by the related ^{15}N-^{1}H correlation time (26, 27). These studies demonstrate the plasticity of the N-terminal region of the PrP, at least in the absence of Cu^{2+}.

Characterization of the conformational properties of proteins at the atomic level by experimental means is challenging and becomes particularly difficult with a process like the conversion of $PrP^C \rightarrow PrP^{Sc}$, which is associated with a substantial conformational change and is accompanied by multimerization. As a result, we use molecular dynamics simulations to complement and extend experiment by simulating PrP^C above and below a pH that triggers conformational changes. Molecular dynamics has become a common technique for simulating the motion of peptides and proteins. The NMR structures offer a great deal of information, and theoretical studies using these structures can provide insight into the conformational flexibility of PrP^C and the impact of changes in pH upon these conformations. In addition, it is not possible experimentally to determine the mechanism of conversion at high resolution. Two short molecular dynamics simulation studies of PrP^C at neutral pH have been reported recently (28, 29). Here we present 10-ns simulations of PrP^C at neutral and low pH and evaluate the connection between low pH and increases in β-structure.

This paper was submitted directly (Track II) to the PNAS office.

Abbreviations: PrP, prior protein; HA, helix A; S1, strand 1; S2, strand 2.

§To whom reprint requests should be addressed. E-mail: daggett@u.washington.edu.

The publication costs of this article were defrayed in part by page charge payment. This article must therefore be hereby marked "*advertisement*" in accordance with 18 U.S.C. §1734 solely to indicate this fact.

Methods

Molecular dynamics simulations beginning with the Syrian hamster NMR structure [1B10, James *et al.* (19), structure #4, residues 109–219, which includes residues implicated in the conformational transition to scrapie] were performed at low (Asp, Glu, and His residues protonated) and neutral/high (above the pKa of His, His neutral) pH in a water box for 10 ns each at 25°C. The solvation shell extended at least 10 Å from any protein atom, resulting in the addition of approximately 6,500 waters. The disulfide bond was left intact, as evidence points to its remaining oxidized in authentic PrP^{Sc} and being necessary for infectivity (30, 31). The simulations were performed with the program ENCAD (32). The protocols and force field have been described (33, 34). A 10-Å force-shifted nonbonded cutoff was used (33). The nonbonded list was updated every two steps. The simulations were performed on Dec EV6 processors. Structures were saved every 0.2 ps for analysis, resulting in 50,000 structures at each pH.

Results and Discussion

From experiment, we expect that PrP^{C} will be stable at neutral pH and will undergo a conformational change at low pH. To address this, simulations were performed, beginning with the hamster NMR structure (residues 109–219) immersed in a box of water molecules. The Cα rms deviations for the neutral pH simulation do indeed remain relatively low (2.1 $\pm$ 0.1 Å from 5–10 ns), whereas the structure deviates more dramatically at low pH (4.7 $\pm$ 0.3 Å, 5–10 ns) (Fig. 1*a*). The heightened mobility of the N-terminal region is evident in the Cα rms fluctuations about the mean structure over the last 2.5 ns of each simulation (Fig. 1*b*). At neutral pH, the fluctuations about the secondary structure are low, and the only high values correspond to the N terminus (residues 109–127) and the loop between helix B and helix C. The low, and quite normal, mobility of the structured part of the molecule is in agreement with hydrogen exchange studies of the human protein (35) and NMR relaxation studies (26, 27). In contrast, high mobility is observed throughout the sequence at low pH, and both the motion and deviations from the starting structure for residues 109–175 [including the N terminus, strand 1 (S1), helix A (HA), and strand 2 (S2)] are striking (Fig. 1*b*). Various snapshots spanning the two simulations are overlaid in Fig. 1*c* to illustrate the nature and extent of the motion.

Examination of structures as a function of time indicates that at neutral pH the protein mostly fluctuates about a mean structure that is very similar to the starting structure (Fig. 1*c*). Interestingly, a short broken helix forms in the unstructured N terminus between residues 110–113 and 117–118 at neutral pH. In contrast, at low pH there are motions spanning many angstroms for residues 109–175 (the front of the protein as depicted in Fig. 2), but the C-terminal helices (helix B and helix C) are stable. The S1 and S2 strands constitute a very short β-sheet in the starting structure (four residues each). However, in the simulation at low pH, both strands elongate to lengthen the sheet. Furthermore, the neighboring unstructured residues (first residues 120–124 and later 110–113) move into the sheet via hydrophobic contacts between side chains (Fig. 2). These changes result in growth of the sheet in both length and width and an increase in the exposure of nonpolar residues (Fig. 2). Residues 121–124 are interesting because they are consistently predicted to form β-structures (36) and the sheet propagated in this region. However, the extended structure is distorted and dynamic and lacks some of the precise packing and hydrogen bonds one would expect in well-behaved β-structures.

In addition, HA and its preceding loop moved by approximately 10–15 Å over the course of the simulation to bring HA into closer proximity to the helix scaffold (Fig. 2). HA experienced some loss of helix at its C terminus to accommodate the movement, and the unfolding of the helix continues over time. The loop appears as if it is moving up to join S2, particularly residues 135–137, which adopt a β-structure (Fig. 2). The shift from helical and turn structures to more extended strands at low pH is illustrated by the distances between the Cα atoms of residue $i \rightarrow i + 3$ (Fig. 3). By 10 ns, five strands form a loosely packed sheet. Interestingly, the short strand comprising residues 137–139 moves 10 Å, and its side chains contact those of S2 (for

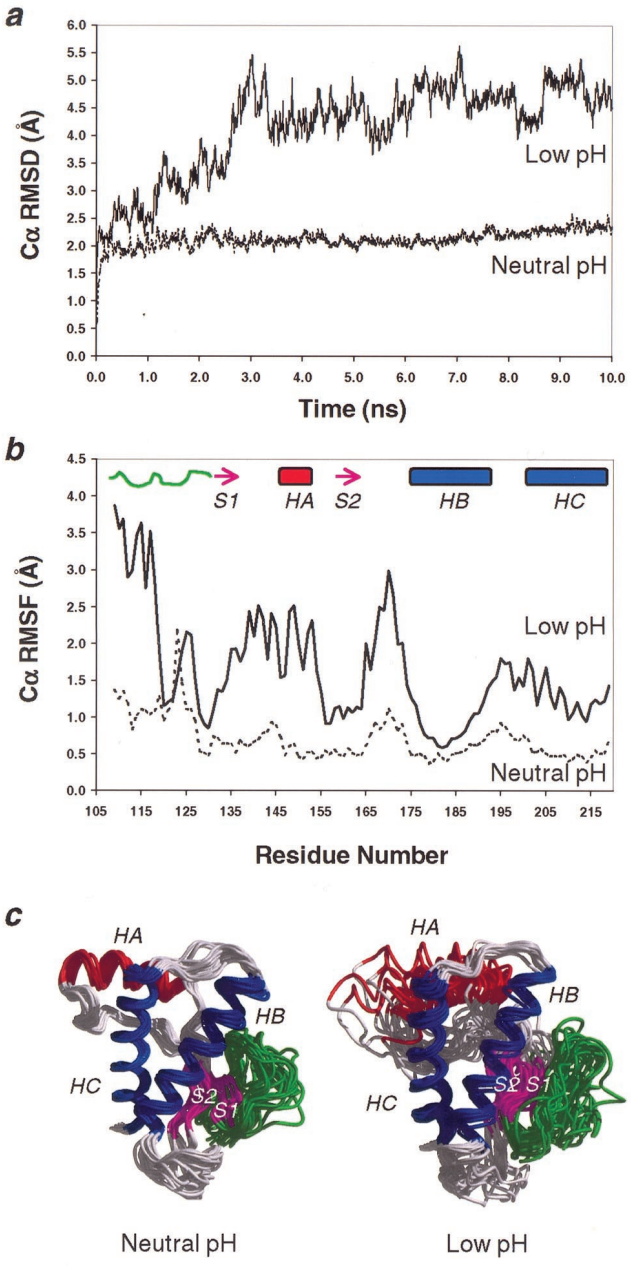

Fig. 1. Molecular dynamics simulations of PrP^{C} at low and neutral pH. (*a*) The rms deviation from the starting NMR structure as a function of simulation time. (*b*) The rms fluctuation of the α-carbons about their mean structure during the last 2.5 ns of the simulations. (*c*) The main chain folds every 0.5 ns over the 10-ns simulations at neutral and low pH. The protein is dynamic, particularly in the turns and loop regions, but the overall structure is well maintained at neutral pH. In contrast, at low pH conformational transitions and fluidity span almost the entire sequence but are particularly prominent at the N terminus and HA.

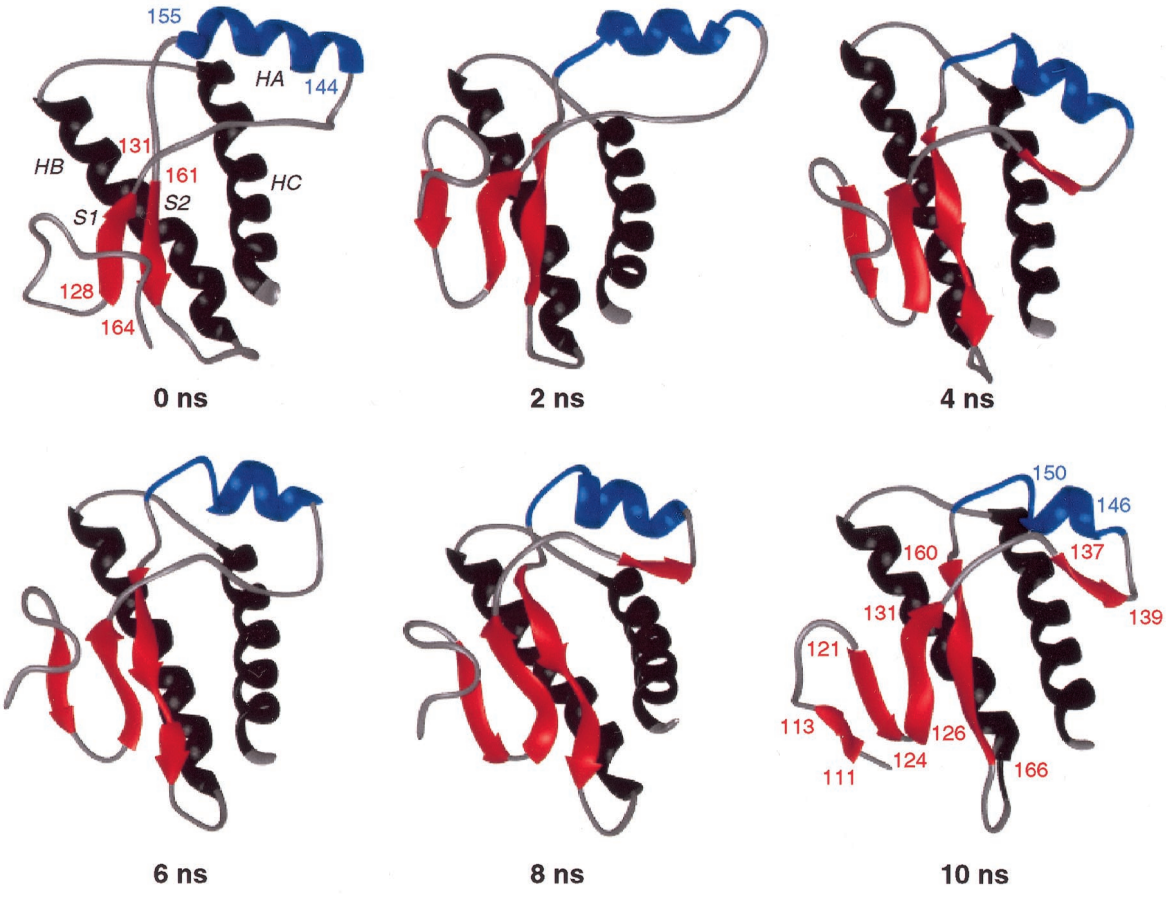

Fig. 2. Temporal history of the simulation of PrP^C at low pH, conditions supporting conformational conversion to PrP^{Sc}. Extension of the β-sheet occurs and the N terminus joins the β-sheet. The residue numbers are labeled for the strands and the helical residues in HA in the first and last structures.

example at 4 ns; Fig. 2). But these interactions are not strong enough to hold the strand down, and it swings toward and away from the rest of the sheet throughout the simulation. Further consolidation of the structure may occur with time. Alternatively, it is possible that the precise β-structure is only obtained upon binding to a PrP^{Sc} molecule, as binding and conversion appear to be separable events (37).

Acid-induced unfolding intermediates have been observed by Swietnicki *et al.* (11) for a human fragment of residues 90–231. They assumed that the bulk of the change involved residues 90–127. However, Hornemann and Glockshuber (12) have also observed an unfolding intermediate of PrP(121–231). So, although the most dramatic changes in the low pH simulation occurred in residues 109–120, the other changes involving residues 135–150 (Fig. 1*c*) are also supported by experiment. The importance of the N-terminal region to conversion is consistent with studies by Peretz *et al.* (38) characterizing the antigenic surfaces of PrP^C and PrP^{Sc}. They found that residues 90–120 are antigenically accessible in PrP^C but are encrypted in PrP^{Sc}. In contrast, residues 220–231 are exposed in both isoforms. Residues in the midregion of the protein show intermediate behavior. A mini-prion can be constructed that contains only residues 89–140 and 177–231, suggesting that one of these two regions is critical to the conformational change but that residues 141–176 are dispensable (39, 40). Moreover, a peptide containing residues 90–144 carrying the P101L mutation folds into a β-rich structure that can cause a prion disease in transgenic mice (41). Because PrP(121–231) is not scrapie competent, residues 90–120 must be of paramount importance.

Why does PrP^C have the potential to undergo this conversion? There are several features that mark the region around S1, S2, and residues 109–127 as potential sites for conversion to β-structure. In the dynamics simulations and NMR studies, residues 109–127 are conformationally heterogeneous and are able to adopt helical, disordered, and more extended conformations. Many residues in this region and around the native β-sheet are already extended in PrP^C but are not actually participating in secondary structural contacts (for example, residues 120–129, 131–144, 155–161, 165, 166). Furthermore, residues 121–124 and 136–141 have the propensity to form β-structure (36). The short existing β-sheet is in close proximity to these residues and appears to serve as a structural nucleus for the formation of new, and propagation of existing, β-like structure (Figs. 2 and 4). In particular, Met-129, which is in S1, rotates away from the β-sheet and pulls the N terminus toward the sheet via interactions with Val-122 (Fig. 4). These interactions remove Val-122 from between the strands and position it out of the hydrogen-bonding plane of the nascent sheet. The native sheet remains intact during this process, but the distance between the N-terminal segment and S1 decreases by >6 Å (Fig. 4). The packing interactions between S1 and S2 also improve, especially between Tyr-128 and Tyr-162, as a result of adding another strand (Fig. 4). This process is an example of tertiary interactions between side chains nucleating secondary structure formation, as has been observed for helix formation in barnase (42). The involvement of Met-129 is interesting because it is a polymorphic site in humans and is associated with variant Creutzfeldt–Jakob disease (3).

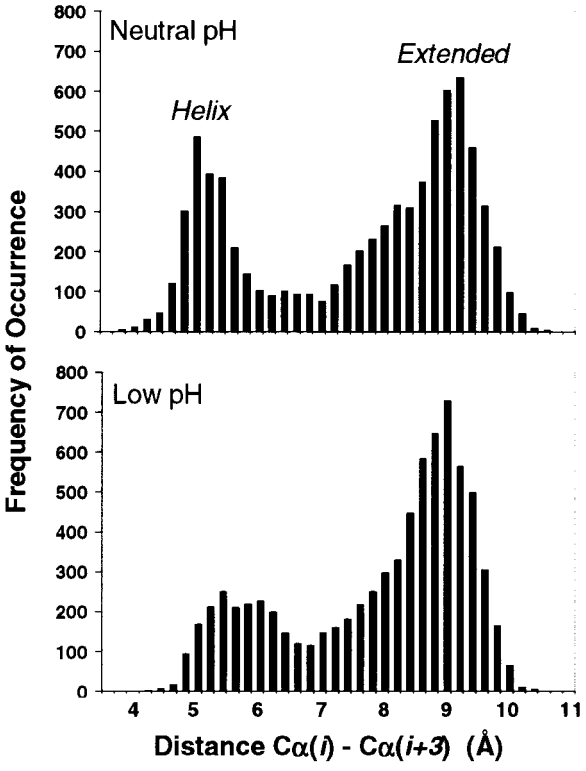

Fig. 3. Histogram of the $C_\alpha(i) \rightarrow C_\alpha(i+3)$ distances for residues 109–172 (i.e., excluding helix B and helix C) from 4 to 10 ns at low and neutral pH. The helical peak drops at low pH, and the amount of extended structure increases.

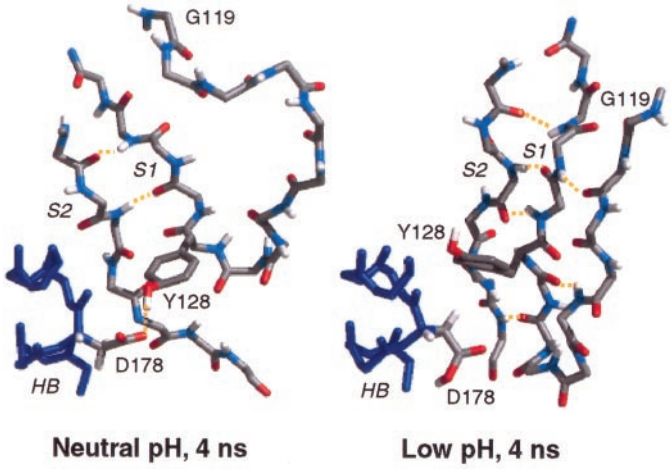

Fig. 5. Role of electrostatic interactions involving Asp-178 in inhibiting conformational changes of PrP^C via interactions with Tyr-128 at neutral pH. Loss of this interaction contributes to changes in the region of the sheet leading to addition of another strand to the β-sheet.

Why are conformational changes facilitated at low pH? Only the protonation states of ionizable residues are altered to define pH in the simulations, without changes in the solvent. To address the role of low pH, the interactions involving the Glu, Asp, and His residues were evaluated in the two simulations. In the neutral pH simulation, Asp-178 forms a charge-stabilized hydrogen bond with Tyr-128 (Fig. 5). However, when this Asp is protonated at low pH, the interaction is broken and Tyr-128 is free to move toward the center of the sheet (Figs. 4 and 5). The first slight movements of the Tyr disrupt its packing with Leu-125, which is initially positioned between the N-terminal segment and the sheet, thereby discouraging addition of the N terminus to the β-sheet. The involvement of Asp-178 is interesting because its mutation to Asn causes fatal familial insomnia or Creutzfeldt–Jakob disease, depending upon whether codon 129 is Met or Val (3). Thus, the neutralization of Asp-178 by mutation to Asn or by protonation appears to favor conversion to PrP^{Sc}.

The results of the molecular dynamics simulation at low pH suggest that this approach can provide insight into the early steps in the conversion of the helix-rich state of PrP^C to PrP^{Sc}, a conformer with increased β-content and diminished helical structure. Various interactions have been described that facilitate or contribute to the changes in conformation, but given the distribution throughout the structure of mutations that cause human disease, we expect that there will also be other specific mechanisms that lead to the same outcome. The simulation of the isolated monomer reflects the tendency of the N-terminal portion of the sequence to convert to β-like structure, but the structure is still far from an idealized β-sheet structure and may

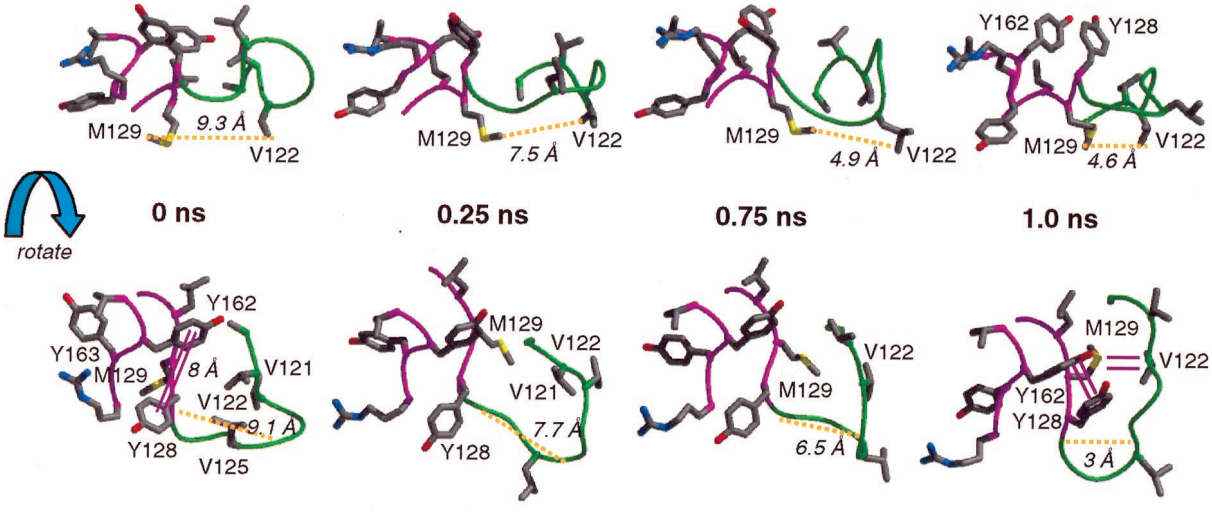

Fig. 4. Addition of the N terminus to the sheet. *Upper*, Met-129 makes interactions with the side chain of Val-122 and pulls the N terminus into the β-sheet. *Lower*, Close-up of N terminus and β-sheet residues.

require intermolecular interactions with another molecule to obtain further consolidation of the sheet. As such, the simulations may be capturing the early steps in the pH-catalyzed transformation to PrP*, an intermediate en route to PrP^{Sc}. With a detailed model of PrP^{Sc}, or an intermediate along the pathway to PrP^{Sc}, we will be in a position to investigate possible binding interactions between PrP^{C} and PrP^{Sc}, to build testable models of PrP^{Sc} aggregates, and to continue structure-based drug design studies (43).

We thank Dr. B. Caughey for helpful discussions. We are grateful for financial support provided by the National Institutes of Health (GM50789 to V.D. and AG02132 to F.E.C.). University of Southern California MIDAS PLUS (44) was used to create the protein displays.

1. Mouillet-Richard, S., Ermonval, M., Chebassier, C., Laplanche, J. L., Lehmann, S., Launay, J. M. & Kellermann, O. (2000) *Science* **289,** 1925–1928.
2. Prusiner, S. B. (1991) *Science* **252,** 1515–1522.
3. Prusiner, S. B. (1998) *Proc. Natl. Acad. Sci. USA* **95,** 13363–13383.
4. DeArmond, S. J. & Prusiner, S. B. (1995) *Am. J. Pathol*. **146,** 785–811.
5. Stahl, N., Baldwin, M. A., Teplow, D. B., Hood, L., Gibson, B. W., Burlingame, A. L. & Prusiner, S. B. (1993) *Biochemistry* **32,** 1991–2002.
6. Caughey, B. W., Dong, A., Bhat, K. S., Ernst, D., Hayes, S. F. & Caughey, W. S. (1991) *Biochemistry* **30,** 7672–7680.
7. Caughey, B. & Raymond, G. J. (1991) *J. Biol. Chem.* **266,** 18217–18223.
8. Pan, K. M., Baldwin, M., Nguyen, J., Gasset, M., Serban, A., Groth, D., Huang, Z., Fletterick, R. J., Cohen, F. E. & Prusiner, S. B. (1993) *Proc. Natl. Acad. Sci. USA* **90,** 10962–10966.
9. Kocisko, D. A., Come, J. H., Priola, S. A., Chesebro, B., Raymond, G. J., Lansbury, P. T. & Caughey, B. (1994) *Nature (London)* **370,** 471–474.
10. Kocisko, D. A., Priola, S. A., Raymond, G. J., Chesebro, B., Lansbury, P. T., Jr. & Caughey, B. (1995) *Proc. Natl. Acad. Sci. USA* **92,** 3923–3927.
11. Swietnicki, W., Petersen, R., Gambetti, P. & Surewicz, W. K. (1997) *J. Biol. Chem*. **272,** 27517–27520.
12. Hornemann, S. & Glockshuber, R. (1998) *Proc. Natl. Acad. Sci. USA* **95,** 6010–6014.
13. Caughey, B., Raymond, G. J., Enrst, D. & Race, R. E. (1991) *J. Virol.* **65,** 6597–6603.
14. Borchelt, D. R., Taraboulos, A. & Prusiner, S. B. (1992) *J. Biol. Chem.* **267,** 6188–6199.
15. Vey, M., Pilkuhn, S., Wille, H., Nixon, R., DeArmond, S. J., Smart, E. J., Anderson, R. G. W., Taraboulos, A. & Prusiner, S. B. (1996) *Proc. Natl. Acad. Sci. USA* **93,** 14945–14949.
16. Kaneko, K., Vey, M., Scott, M., Pilkuhn, S., Cohen, F. E. & Prusiner, S. B. (1997) *Proc. Natl. Acad. Sci. USA* **94,** 2333–2338.
17. Anderson, R. G. W. (1998) *Annu. Rev. Biochem*. **26,** 199–225.
18. Riek, R., Hornemann, S., Wider, G., Billeter, M., Glockshuber, R. & Wüthrich, K. (1996) *Nature (London)* **382,** 180–182.
19. James, T. L., Liu, H., Ulyanov, N. B., Farr-Jones, S., Zhang, H., Donne, D., Kaneko, K., Groth, D., Mehlhorn, I., Prusiner, S. B., *et al.* (1997) *Proc. Natl. Acad. Sci. USA* **94,** 10086–10091.
20. Liu, H., Farr-Jones, S., Ulyanov, N. B., Llinas, M., Marqusee, S., Groth, D., Cohen, F. E., Prusiner, S. B. & James, J. T. (1999) *Biochemistry* **38,** 5362–5377.
21. Zahn, R., Liu, A., Luhrs, T., Riek, R., von Schroetter, C., Lopez Garcia, F., Billeter, M., Calzolai, L., Wider, G. & Wuthrich, K. (2000) *Proc. Natl. Acad. Sci. USA* **97,** 145–150.
22. Viles, J. H., Cohen, R. E., Prusiner, S. B., Goodin, D. B., Wright, P. E. & Dyson, H. J. (1999) *Proc. Natl. Acad. Sci. USA* **96,** 2042–2047.
23. Whittal, R. M., Ball, H. L., Cohen, R. E., Burlingame, A. L., Prusiner, S. B. & Baldwin, M. A. (2000) *Protein Sci*. **9,** 332–343.
24. Morillas, M., Swietnicki, W., Gambetti, P. & Surewicz, W. K. (1999) *J. Biol. Chem*. **274,** 36859–36865.
25. Kanyo, Z. F., Pan, K.-M., Williamson, A., Burton, D. R., Prusiner, S. B., Fletterick, R. J. & Cohen, F. E. (1999) *J. Mol. Biol.* **293,** 855–863.
26. Riek, R., Hornemann, S., Wider, G., Glockshuber, R. & Wuthrich, K. (1997) *FEBS Lett*. **413,** 282–288.
27. Donne, D. G., Viles, J. H., Groth, D., Mehlhorn, I., James, J. L., Cohen, F. E., Prusiner, S. B., Wright, P. E. & Dyson, H. J. (1997) *Proc. Natl. Acad. Sci. USA* **94,** 13452–13457.
28. Zuegg, J. and Gready, J. E. (1999) *Biochemistry* **38,** 13862–13876.
29. Parchment, O. G. & Essex, J. W. (2000) *Proteins Struct. Funct. Genet*. **38,** 327–340.
30. Turk, E., Teplow, D. B., Hood, L. E. & Prusiner, S. B. (1998) *Eur. J. Biochem*. **176,** 21–30.
31. Hermann, L. M. & Caughey, B. (1998) *NeuroReport* **9,** 2457–2461.
32. Levitt, M. (1990) *ENCAD: Energy Calculations and Dynamics,* ed. Molecular Applications Group (Stanford University, Palo Alto, CA, and Yeda, Rehovot, Israel).
33. Levitt, M., Hirshberg, M., Sharon, R. & Daggett, V. (1995) *Comp. Phys. Comm.* **91,** 215–231.
34. Levitt, M., Hirshberg, M., Sharon, R., Laidig, K. E. & Daggett, V. (1997) *J. Phys. Chem. B* **101,** 5051–5061.
35. Hosszu, L. L. P., Baxter, N. J., Jackson, G. S., Power, A., Clarke, A. R., Waltho, J. P., Craven, C. J. & Collinge, J. (1999) *Nat. Struct. Biol*. **6,** 740–743.
36. Alonso, D. O. V. & Daggett, V. (2001) *Adv. Protein Chem*. **57,** 107–137.
37. Horiuchi, M. & Caughey, B. (1999) *EMBO J.* **18,** 3193–3203.
38. Peretz, D., Williamson, R. A., Matsunaga, Y., Serban, H., Pinilla, C., Bastidas, R. B., Rozenshteyn, R., James, T. L., Houghten, R. A., Cohen, F. E., *et al.* (1997) *J. Mol. Biol*. **273,** 614–622.
39. Supattapone, S., Bosque, P., Muramoto, T., Wille, H., Aagaard, C., Peretz, D., Nguyen, H.-O.B., Heinrich, C., Torchia, M., Safar, J., *et al.* (1999) *Cell* **96,** 896–878.
40. Baskakov, I. V., Aagaard, C., Mehlhorn, I., Wille, H., Groth, D., Baldwin, M. A., Prusiner, S. B. & Cohen, F. E. (2000) *Biochemistry* **39,** 2792–2804.
41. Kaneko, K., Ball, H. L., Wille, H., Zhang, H., Groth, D., Torchia, M., Tremblay, P., Safar, J., Prusiner, S. B., DeArmond, S. J., *et al.* (2000) *J. Mol. Biol.* **295,** 997–1007.
42. Wong, K. B., Clarke, J., Bond, C. J., Neira, J. L., Freund, S. M. V., Fersht, A. R. F. & Daggett, V. (2000) *J. Mol. Biol*. **296,** 1257–1282.
43. Perrier, V., Wallace, A. C., Kaneko, K., Safar, J., Prusiner, S. B. & Cohen, F. E. (2000) *Proc. Natl. Acad. Sci. USA* **97,** 6073–6078.
44. Ferrin, T. E., Huang, C. C., Jarvis, L. E. & Langridge, R. (1988) *J. Mol. Graphics* **6,** 13–27.